frontiers | Frontiers in Physics

TYPE Original Research
PUBLISHED 17 October 2022
DOI 10.3389/fphy.2022.1014644

OPEN ACCESS

EDITED BY
Animasaun I. L.,
Federal University of Technology, Nigeria

REVIEWED BY
Sanatan Das,
University of Gour Banga, India
Mohammed Shamshuddin,
Vaagdevi College of Engineering, India
Mahanthesh B.,
Christ University, India

*CORRESPONDENCE
Aisha M. Alqahtani,
Alqahtani@pnu.edu.sa

SPECIALTY SECTION
This article was submitted to Interdisciplinary Physics, a section of the journal Frontiers in Physics

RECEIVED 08 August 2022
ACCEPTED 07 September 2022
PUBLISHED 17 October 2022

CITATION
Naveed Khan M, Alhowaity S, Wang Z, Alqahtani AM, Tag-eldin E and Yassen MF (2022), Significance of multiple solutions on the dynamics of ethylene glycol conveying gold and copper nanoparticles on a shrinking surface.
Front. Phys. 10:1014644.
doi: 10.3389/fphy.2022.1014644

Significance of multiple solutions on the dynamics of ethylene glycol conveying gold and copper nanoparticles on a shrinking surface

Muhammad Naveed Khan[1], Sawsan Alhowaity[2], Zhentao Wang[3], Aisha M. Alqahtani[4]*, Elsayed Tag-eldin[5] and Mansour F. Yassen[6,7]

[1]Department of Mathematics, Quaid-i-Azam University, Islamabad, Pakistan, [2]Department of Mathematics, Shaqra University, Shaqra, Saudi Arabia, [3]School of Energy and Power Engineering, Jiangsu University, Zhenjiang, China, [4]Department of Mathematical Sciences, College of Science, Princess Nourah bint Abdulrahman University, Riyadh, Saudi Arabia, [5]Faculty of Engineering and Technology, Future University in Egypt, New Cairo, Egypt, [6]Department of Mathematics, College of Science and Humanities in Al-Aflaj, Prince Sattam Bin Abdulaziz University, Al-Kharj, Saudi Arabia, [7]Department of Mathematics, Faculty of Science, Damietta University, Damietta, Egypt

All previously published data on the dynamics of ethylene glycol conveying copper and gold nanoparticles over a convective surface, nothing is known about the importance of dual branch solutions. Hybrid nanofluids improve the thermal conductivity of the fluid. The nanoparticles copper and gold having ethylene glycol as a base fluid are used here. The flow problem is described over a stretching/shrinking surface with the influence of Ohmic heating, non-linear radiation, and a convectively heated surface. Furthermore, the magnetic field strength is applied perpendicular to the direction of the flow. To control the fluid, flow-governing equations are numerically solved by using bvp4c, a built-in approach in MATLAB. For hybrid nanomaterials, the consequence of different physical parameters is discussed graphically and with tabular data. A comparison with previous findings reveals that the present findings are in good agreement. The results revealed that the coefficient of skin friction for the physically stable branch declines over a certain range of shrinking parameters; nonetheless, for the unstable branch, the reverse pattern is discovered. The magnetic force diminishes the flow field and energy dispersion in the upper branch but improves it in the lower branch.

KEYWORDS

stretching/shrinking surface, stagnation-point flow, non-linear thermal radiation, hybrid nanomaterials, dual solution

1 Introduction

In industries, heat transfer is used in a wide range of applications to lower and raise temperatures. The conditions for energy exchange in a system are provided by heat transfer fluids, and the effects of these fluids depend on their physical characteristics, including thermal conductivity, viscosity, density, and heat capacity. The low thermal conductivity of typical fluids such as water, ethylene glycol, or oil cannot achieve significant heat exchange rates in thermal engineering equipment. To overcome this barrier, ultrafine solid particles contained in ordinary fluids can be used to improve their thermal conductivity. A nanofluid is defined as a suspension of nano-sized particles in a regular base fluid. In the formulation of the nanofluids, usually metals, carbon nanotubes, and carbides as nanoparticles are utilized. The metal nanoparticles incorporate gold and silver while copper oxide, zinc oxide, and aluminum oxide are included into the category of oxide nanoparticles. In comparison to suspensions with millimeter- or micrometer-sized particles, nanofluids exhibit greater stability, rheological characteristics, and significantly higher thermal conductivities [1]. In modern technology, the use of nanofluids is to promote system miniaturization by lowering particle clogging. Numerous researchers have recently examined, both experimentally and theoretically, how nanofluids can improve heat transmission in thermal engineering devices. In order to calculate the thermophysical properties of nanofluids, researchers have used a range of preparation techniques, features, and models. Choi [2] developed the idea of nanofluids by suggesting that nanoparticles be suspended in a base fluid. Following that, several researchers studied the heat transport of a nanofluid for various aspects, either experimentally or numerically. For instance, Tiwari and Das [3] reported their work on the mathematical models of nanofluids. The efficiency of particle micromixing in heavy metal reduction procedures under different inlet conditions was covered by Karvelas et al. [4]. Benos et al. [5] discussed the theoretical model for natural convection of the CNT–water nanofluid flow that incorporates the revised Hamilton–Crosser model. Kouz et al. [6] presented the analysis of the heat transfer and entropy generation of a water–Fe_3O_4/CNT hybrid magnetic nanofluid flow in a trapezoidal wavy enclosure with porous media. Song et al. [7] considered a convectively heated vertical surface to examine the nanofluid influenced by a haphazard motion with the Buongiorno model. The hydromagnetic flow phenomenon of the Casson nanofluid with the involvement of an exponentially shrunk sheet was scrutinized by Ishtiaq and Nadeem [8]. Many researchers have used the Tiwari–Das nanofluid model to examine many aspects of the flow, including in Ref. [9–26].

Thermal radiation's effect on heat transfer is becoming increasingly significant in the design of modern energy conversion systems that operate at high temperatures. Furthermore, thermal radiation is used to solve a wide range of technological difficulties, including combustion, nuclear reactor safety, solar collectors, and furnace design. A nanofluid has distinct features than either particles or the base fluid, so studying the effects of thermal radiation on the flow and heat transfer characteristics in a nanofluid has garnered a lot of attention. Due to this fact, numerous researchers have investigated the effects of thermal radiation on the flow, heat transfer, and other different features in a nanofluid. In a single-phase model, Hady et al. [27] investigated the boundary layer viscous flow and heat transfer properties of a nanofluid across a nonlinearly stretching sheet in the presence of thermal radiation. Mahanthesh et al. [28] investigated the radiative flow of the water-based nanofluid over a convectively heated surface. Shoaib et al. [29] numerically investigated the rotational flow of the magnetized hybrid nanofluid with radiation effects across a stretching sheet. Mabood et al. [30] discussed the irreversibility analysis in hybrid nanomaterials with nonlinear thermal radiation and melting heat transfer. Jamaludin et al. [31] explored the stagnation-point flow of a nanofluid due to a stretching/shrinking surface in the existence of thermal radiation, suction, and a heat source/sink. The comparative analysis for the radiative flow of hybrid nanomaterials and nanomaterials in a permeable porous medium was performed by Yasir et al. [32]. Very recently, Yasir et al. [33] further explored the dynamics of ethylene glycol transporting copper and titania nanoparticles on a curved object in the presence of nonlinear thermal radiation and a heat source/sink. The interesting articles that depend on heat transport through nanoparticles are in Ref. [34–44].

The existing examination is being held out to explore the radiative stagnation-point flow of hybrid nanomaterials subject to a permeable shrinking surface. As evidenced by the literature, investigation of the hybrid nanofluid stagnation-point flow is uncommon. In this scenario, gold and copper are mixed into the ethylene glycol base fluid to formulate a hybrid nanofluid that implements a stagnation-point flow mechanism on a shrinking sheet. Furthermore, the association between the aligned magnetic field and wall suction was scrutinized. The shooting technique was used to solve the resulting nonlinear ordinary differential equations, and the solution was calculated in terms of velocity, temperature, local Nusselt number, and skin friction coefficient, all of which are dictated by relevant flow parameters. In our perspective, we have extremely competitively investigated this problem. The several originalities of the current analysis are emphasized as follows:

(a) To efficiently manage the flow, the boundary layer separation points for various control parameters are shown.
(b) It is observed that the suitable amount of control parameters improved the rates of skin friction and heat transfer.
(c) What is the consequence of gold and copper nanoparticles on the thermal conductivity of ethylene glycol over a shrinking surface?

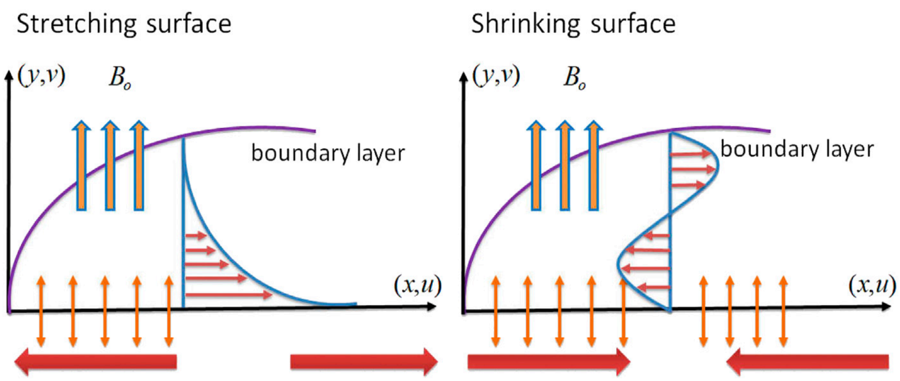

FIGURE 1
Flow diagram.

2 Mathematical formulation

In the presence of a porous medium, the magnetized flow of a hybrid nanofluid over a permeable shrinking surface is considered. The physical coordinate system is depicted in Figure 1, where the $x-$ axis is measured along the surface and the $y-$ axis is normal to it. The hypothesis is that the velocity of the shrinking surface is $u_w(x) = cx$ and the free-stream velocity is $u_e(x) = ax$. Furthermore, the surface temperature is T_w, while the ambient hybrid nanomaterial temperature is T_∞. Tiwari and Das' mathematical nanofluid model was used in this study. To investigate the thermal transport of a hybrid nanofluid, Ohmic heating and viscous dissipation with nonlinear thermal radiation over a convectively heated surface are taken into account.

The model equations for hybrid nanomaterials are as follows:

$$\frac{\partial u}{\partial x} + \frac{\partial v}{\partial y} = 0, \tag{1}$$

$$u\frac{\partial u}{\partial x} + v\frac{\partial u}{\partial y} = ue\frac{du_e}{dx} + \frac{\mu_{hnf}}{\rho_{hnf}}\frac{\partial^2 u}{\partial y^2} - \frac{\sigma_{hnf} B_o^2 (u - u_e)}{\rho_{hnf}} - \frac{\mu_{hnf}}{\rho_{hnf}}\frac{(u - u_e)}{k^*}, \tag{2}$$

$$u\frac{\partial T}{\partial x} + v\frac{\partial T}{\partial y} = \frac{k_{hnf}}{(\rho c_p)_{hnf}}\frac{\partial^2 T}{\partial y^2} - \frac{1}{(\rho c_p)_{hnf}}\frac{\partial q_r}{\partial y} + \frac{\mu_{hnf}}{(\rho c_p)_{hnf}}\left(\frac{\partial u}{\partial y}\right)^2 + \frac{\sigma_{hnf} B_o^2}{(\rho c_p)_{hnf}}(u - u_e)^2. \tag{3}$$

The related boundary conditions are as follows:

$$\left.\begin{array}{c} u = u_w(x),\ v = v_w(x) \text{ and } -k_{hnf}\dfrac{\partial T}{\partial y} = h(T_w - T) \text{ at } y = 0 \\ u \to u_e(x) \text{ and } T \to T_\infty \text{ as } y \to \infty \end{array}\right\}, \tag{4}$$

where v and u symbolize the hybrid nanomaterial velocity components along the y and x directions, respectively. T is the fluid temperature, v_w signifies the velocity mass flux, and the radiative heat flux q_r is defined as follows:

$$q_r = \frac{-16\sigma^*}{3k^*}T^3\frac{\partial T}{\partial y}, \tag{5}$$

in which $k*$ symbolizes the Stefan–Boltzmann constant and $\sigma*$ represents the mean absorption coefficient.

Letting

$$u = axf'(\eta),\ v = -(av_f)^{\frac{1}{2}} f(\eta),\ \theta = \frac{T - T_\infty}{T_w - T_\infty},\ \eta = \sqrt{\frac{a}{\nu_f}}y, \tag{6}$$

which converts the governing Eqs. 2–4 as

$$\frac{\mu_{hnf}/\mu_f}{\rho_{hnf}/\rho_f}f''' + ff'' - f'^2 + M\frac{\sigma_{hnf}/\sigma_f}{\rho_{hnf}/\rho_f}(1 - f') + k_p\frac{\mu_{hnf}/\mu_f}{\rho_{hnf}/\rho_f}(1 - f') + 1 = 0, \tag{7}$$

$$\left.\begin{array}{l} \dfrac{1}{\Pr}\dfrac{k_{hnf}/k_f}{(\rho c_p)_{hnf}/(\rho c_p)_f}\theta'' + \dfrac{4}{3}R_d\left[\theta''\{1 + (\theta_w - 1)\theta\}^3 + 3(\theta_w - 1)\theta'^2\{1 + (\theta_w - 1)\theta\}^2\right] \\ + f\theta' + \dfrac{1}{(\rho c_p)_{hnf}/(\rho c_p)_f}\left\{\dfrac{\mu_{hnf}}{\mu_f}Ecf''^2 + \dfrac{\sigma_{hnf}}{\sigma_f}MEc(1 - f')^2\right\} = 0 \end{array}\right\}, \tag{8}$$

with boundary conditions

$$\left.\begin{array}{c} f(\eta) = S,\ f'(\eta) = \chi,\ -\dfrac{k_{hnf}}{k_f}\theta'(0) = \beta_i\{1 - \theta(0)\}, \\ f'(\eta) \to 1,\ \theta(\eta) \to 0 \text{ as } \eta \to \infty \end{array}\right\}. \tag{9}$$

Here, $\chi(=\frac{c}{a})$ is the constant stretching/shrinking parameter, $M(=\frac{\sigma B_o^2}{a\rho_f})$ is the magnetic field, $S(=-\frac{v_w}{\sqrt{a\nu_f}})$ is the mass flux

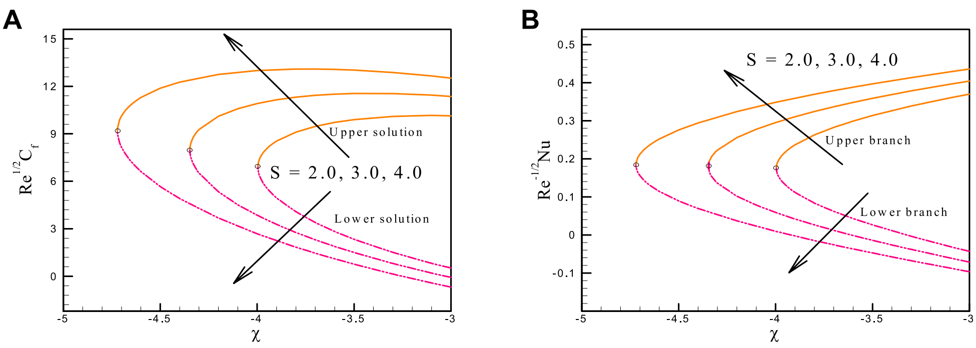

FIGURE 2
Interpretation of $Re^{\frac{1}{2}}C_f$ and $Re^{-\frac{1}{2}}Nu$ for distant values of S.

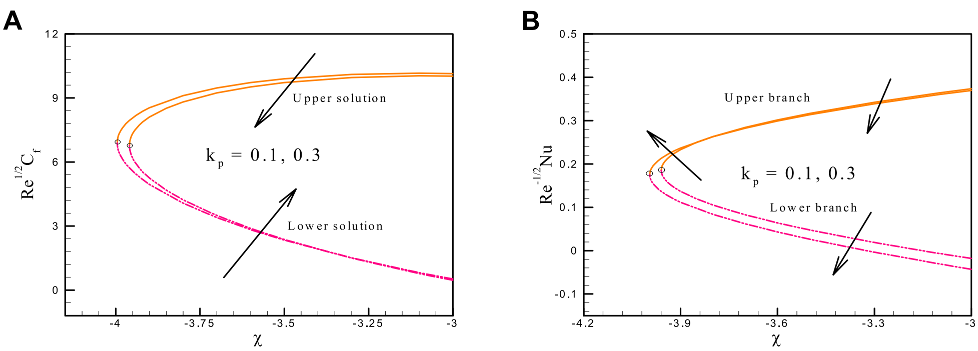

FIGURE 3
Interpretation of $Re^{\frac{1}{2}}C_f$ and $Re^{-\frac{1}{2}}Nu$ for distant values of k_p.

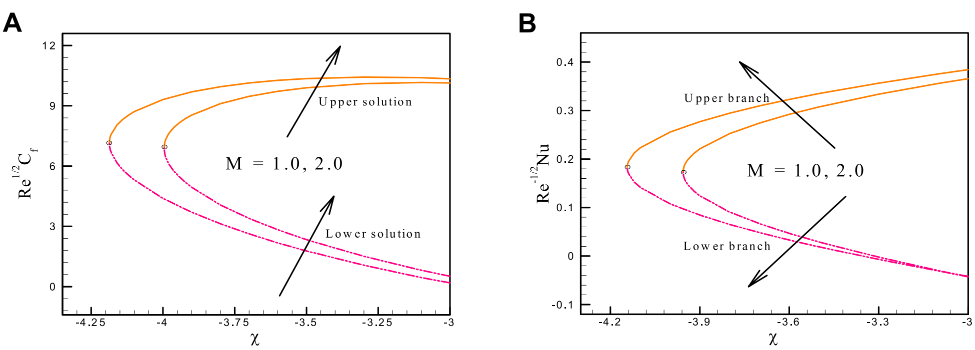

FIGURE 4
Interpretation of $Re^{\frac{1}{2}}C_f$ and $Re^{-\frac{1}{2}}Nu$ for distant values of M.

constant, $k_p\left(=\frac{\nu_f}{k_p^* U_\infty}\right)$ is the porous media permeability parameter, $\Pr\left(=\frac{\nu_f \rho c_p}{k_f}\right)$ is the Prandtl number, $\theta_w\left(=\frac{T_w}{T_\infty}\right)>1$ is the temperature ratio parameter, $Ec\left(=\frac{u_e^2}{c_p(T_w-T_\infty)}\right)$ is the Eckert number, $R_d\left(=\frac{4\sigma^* T_\infty^3}{k^* k_f}\right)$ is the thermal radiation, and $\gamma\left(=\frac{h}{k_f}\sqrt{\frac{\nu_f}{a}}\right)$ is the Biot number.

The skin friction coefficient C_f and heat transfer rate Nu_x are expressed as

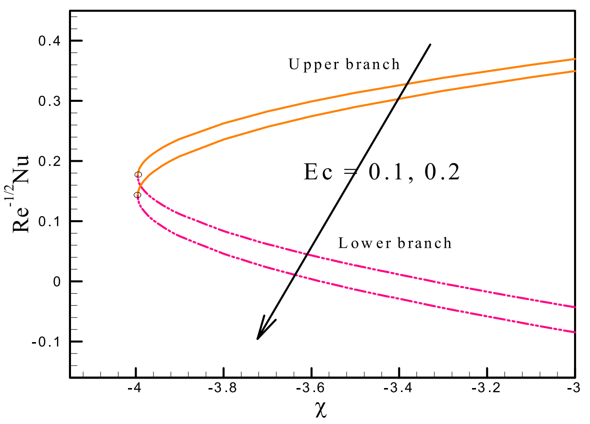

FIGURE 5
Interpretation of $\mathrm{Re}^{-\frac{1}{2}}Nu$ for distant values of Ec.

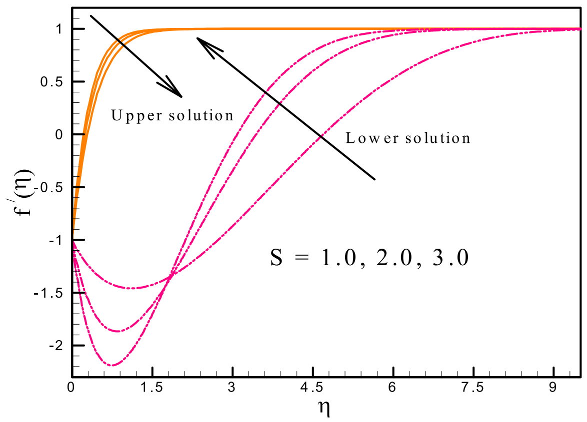

FIGURE 7
Interpretation of $f'(\eta)$ for ϕ_1 values of S.

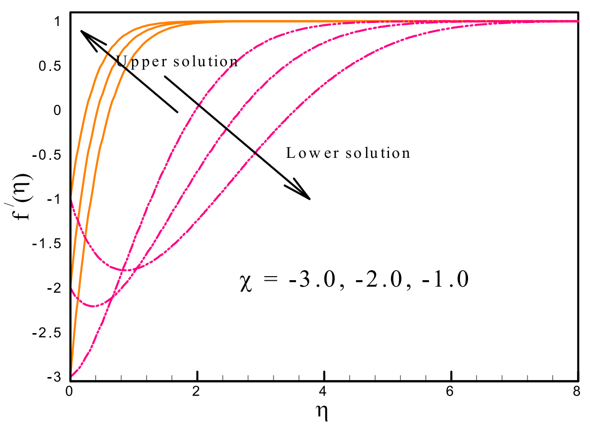

FIGURE 6
Interpretation of $f'(\eta)$ for distant values of χ.

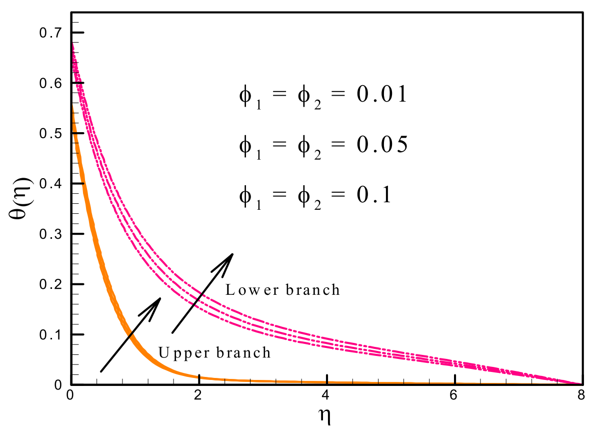

FIGURE 8
Interpretation of $\theta(\eta)$ for distant values of ϕ_1 and ϕ_2.

$$C_f = \frac{\tau_w}{\rho_f u_e^2},\ Nu_x = \frac{x q_w}{k_f (T_w - T_\infty)}, \tag{10}$$

where τ_w and q_w are defined as

$$\tau_w = \mu_{hnf}\left(\frac{\partial u}{\partial y}\right)\bigg|_{y=0},\ q_w = -k_{hnf}\left(\frac{\partial T}{\partial y}\right)\bigg|_{y=0} + q_r\big|_{y=0}. \tag{11}$$

By using equation (11), the dimensionless form of the equation (10) is

$$\left.\begin{aligned} \mathrm{Re}^{\frac{1}{2}} C_{f_x} &= \frac{\mu_{hnf}}{\mu_f} f''(0) \\ \mathrm{Re}^{-\frac{1}{2}} Nu_x &= -\frac{k_{hnf}}{k_f}\left\{1 + \frac{4}{3}R_d\left(1 + (\theta_w - 1)\theta(0)\right)^3\right\}\theta'(0) \end{aligned}\right\}, \tag{12}$$

where $\mathrm{Re}\left(= \frac{u_e(x)}{\nu_f}\right)$ is the local Reynolds number; μ_{hnf}, ρ_{hnf}, k_{hnf}, $(\rho c_p)_{hnf}$, and σ_{hnf} are the hybrid nanomaterials' dynamic viscosity, effective density, thermal conductivity, heat capacity, and electrical conductivity, respectively, which are defined as [45]. Further, the thermo-physical properties also defined in Table 1,

$$\left.\begin{aligned} \rho_{hnf} &= (1-\phi_2)\left((1-\phi_1)\rho_f + \rho_1\phi_1\right) + \phi_2\rho_2 \\ \mu_{hnf} &= \frac{\mu_f}{(1-\phi_1)^{2.5}(1-\phi_2)^{2.5}},\ \nu_{hnf} = \frac{\mu_{hnf}}{\rho_{hnf}} \\ k_{hnf} &= k_{bf}\left\{\frac{k_2 + (n-1)k_{bf} - (n-1)(k_{bf} - k_2)\phi_2}{k_2 + (n-1)k_{bf} + (k_{bf} - k_2)\phi_2}\right\},\ k_{bf} = k_f\left\{\frac{k_1 + (n-1)k_f - (n-1)(k_f - k_1)\phi_1}{k_1 + (n-1)k_f + (k_f - k_1)\phi_1}\right\} \\ (\rho c_p)_{hnf} &= (1-\phi_2)\left((1-\phi_1)(\rho c_p)_f + (\rho c_p)_1\phi_1\right) + \phi_2(\rho c_p)_2 \\ \sigma_{hnf} &= \sigma_{bf}\left\{\frac{\sigma_2(1+2\phi_2) + 2\sigma_{bf}(1-\phi_2)}{\sigma_2(1-\phi_2) + \sigma_{bf}(2+\phi_2)}\right\},\ \sigma_{bf} = \sigma_f\left\{\frac{\sigma_1(1+2\phi_1) + 2\sigma_f(1-\phi_1)}{\sigma_1(1-\phi_1) + \sigma_f(2+\phi_1)}\right\} \end{aligned}\right\}. \tag{13}$$

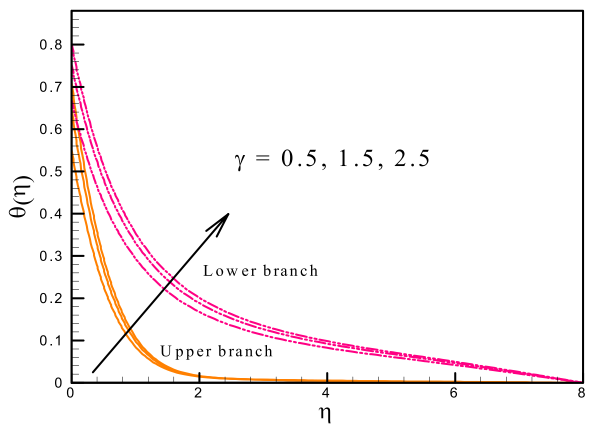

FIGURE 9
Interpretation of $\theta(\eta)$ for distant values of γ.

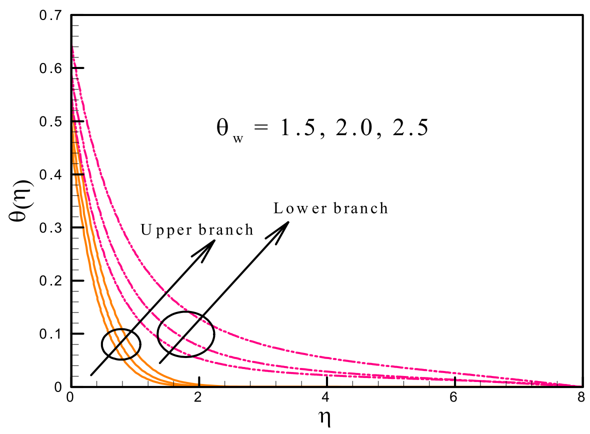

FIGURE 11
Interpretation of $\theta(\eta)$ for distant values of θ_w.

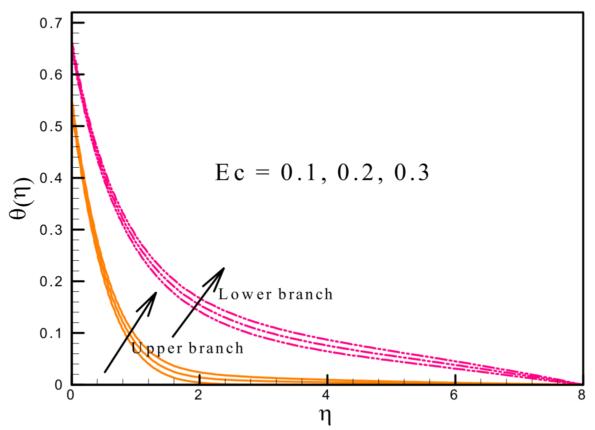

FIGURE 10
Interpretation of $\theta(\eta)$ for distant values of Ec.

3 Graphical analysis

This study's objectives include the following: (i) investigating the effects of relevant parameters on the flow and heat transfer; (ii) detecting the existence of dual solutions; and (iii) verifying the nature of the solution. As a result, the outcomes and discussions regarding the goal will be clarified in this part. The numerical solution is determined using the following control parameters: The results are presented in a graphical style to provide a better understanding of the effect of the physical parameter. The variation of $\mathrm{Re}^{\frac{1}{2}}C_f$ and $\mathrm{Re}^{-\frac{1}{2}}N_u$ against χ with the interpretation of S are portrayed in Figures 2A, B. According to these figures, solutions exist in the range $\chi_c < \chi$ for hybrid nanomaterials, but no solution occurs beyond the turning points, that is, when $\chi < \chi_c$. The region's outcome route clearly widens as the value of S increases, with the bifurcation values of χ_c. Furthermore, in the physically stable branch of the solution, the skin friction coefficient increases, whereas in the unstable branch, the opposite tendency is observed. As the porous medium is taken into account in this model, so Figures 3A, B depict the fluctuation of $\mathrm{Re}^{\frac{1}{2}}C_f$ and $\mathrm{Re}^{-\frac{1}{2}}N_u$ against the shrinking parameter χ with different values of the porosity parameter $k_p (= 0.1, 0.3)$. It is seen that the boundary layer bifurcates at the crucial points $\chi_c = -3.9592$ at $k_p (= 0.1)$ and $\chi_c = -3.9954$ at $k_p (= 0.3)$. This also implies that increasing the porosity parameter k_p delays the bifurcation process. As a result of the increased porosity parameter k, the skin friction coefficient $\mathrm{Re}^{\frac{1}{2}}C_f$ decreases for the upper solution and increases for the lower branch solution, while the local Nusselt number $\mathrm{Re}^{-\frac{1}{2}}N_u$ shows a decline trend. Furthermore, the rising behavior of the magnetic field parameter M on $\mathrm{Re}^{\frac{1}{2}}C_f$ and $\mathrm{Re}^{-\frac{1}{2}}Nu$ is depicted in Figures 4A, B. The magnetic field is influenced more by the dispersion of Au nanoparticles in the nanofluid. The rate of heat transfer increases with the concentration of nanoparticles because intermolecular collisions increase the kinetic energy. Additionally, the skin friction coefficient demonstrates a similar impact. Figure 5 shows the influence of the Eckert number Ec on $\mathrm{Re}^{-\frac{1}{2}}Nu$ in the direction of χ. In the first and second solutions, raising Ec slows down the rate of heat transportation. However, the uncertainty in the boundary layer partition is unaffected by the increasing Eckert number. As a result, the dual branches are only applicable up to the identical critical value for all Ec values. Figure 6 represents the effects of shrinking velocity on the dimensionless velocity profile. It is observed that the velocity profile significantly decreases with shrinking velocity for the upper branch solution, while increases for the lower branch solution. The physical importance of this problem shows that in the case of dual solutions, the flow separates from the plate, which is very important for many practical problems. The fluctuation of the mass suction

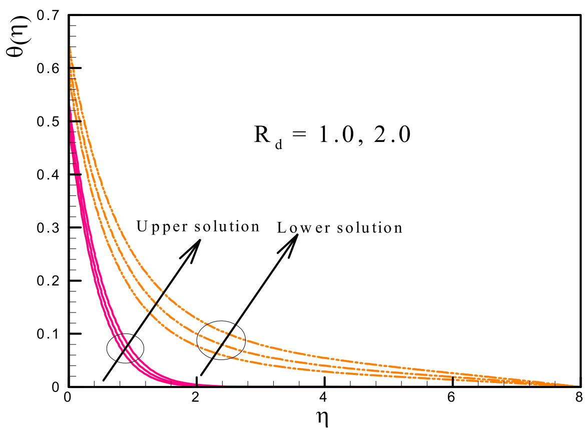

FIGURE 12
Interpretation of $\theta(\eta)$ for distant values of δ.

parameter S on the velocity profile in relation to the similarity variable η is shown in Figure 7. Here, it is noted that suction diminishes the thickness of the related boundary layer due to the physical increase in velocity distribution. Figure 8 depicts the effect of the volume percentage of nanoparticles on the temperature distribution. Because of an upsurge in the kinetic energy of the system, the fluid temperature inclines. This increase in kinetic energy promotes thermal transfer. Figure 9 demonstrates the influence of γ on the temperature distribution. The Biot number improves the temperature of the fluid in consort with the boundary layer thickness. In actuality, increasing the Biot number improves the penetration depth. To study the behavior of thermal distribution for distinct values of Ec,Figure 10 is sketched. Since Ec is derived from the appearance of the Joule heating result, the increment in Ec also indicates that a stronger heat generation from the electric current reference has been considered to the conducting sheet, which therefore generates the upgrade in temperature. Figure 11 is sketched to analyze the nature of temperature distribution $\theta(\eta)$ for various values of $\theta_w\,(= 1.5, 2.0, 2.5)$. It is found that the fluid temperature $\theta(\eta)$ and the associated thickness, both are enhanced on increasing θ_w. Figure 12 shows the effect of thermal radiation on $\theta(\eta)$, and it can be seen from this figure that $\theta(\eta)$ rises as R_d is increased. This is because as R_d is increased, the fluid absorbs more heat, causing a rise in $\theta(\eta)$.

The numerical outputs of the existing analysis with those reported in Ref. [45] for distinct values of the shrinking parameter are scrutinized, and the outcomes are demonstrated in Table 2. The obtained results are extremely compact, providing confidence in the current procedure's validity.

4 Numerical solution procedure

By permitting the following condition to exist, we performed the procedure:

$$\left.\begin{array}{c} f = \xi_1,\ f' = \xi_2,\ f'' = \xi_3,\ f''' = \xi\xi_1, \\ \theta = \xi_4,\ \theta' = \xi_5,\ \theta'' = \xi\xi_2 \end{array}\right\}, \tag{14}$$

TABLE 1 Thermo-physical properties of the base fluid and nanoparticles [33, 45].

Physical property	Nanoparticles		Base fluid
	Gold (Au)	Copper (Cu)	Ethylene glycol
$c_p\,(J/kg\ K)$	$c_{p_1} = 129$	$c_{p_2} = 385$	2430
$k\,(W/m\ K)$	$k_1 = 318$	$k_2 = 401$	0.253
$\rho\,(kg/m^3)$	$\rho_1 = 19300$	$\rho_2 = 8933$	1115
Pr	—	—	2.0363

TABLE 2 Comparison of $Re^{\frac{1}{2}}C_{fx}$ for distant values of χ.

χ	Hafeez et al. [46]		Current results	
	Upper solution	Lower solution	Upper solution	Lower solution
−0.25	1.4022331	—	1.4021311	—
−0.50	1.4958565	—	1.4947538	—
−0.75	1.4893224	—	1.4893124	—
−1.00	1.3281191	0	1.3287901	—
−1.15	1.0823058	0.1160042	1.0824134	0.1166937
−1.20	0.9320782	0.2336751	0.9325191	0.2334401

$$\xi\xi_1 = -\frac{\rho_{hnf}/\rho_f}{\mu_{hnf}/\mu_f}\left\{\xi_1\xi_3 + \xi_2^2\right\} - M\frac{\sigma_{hnf}/\sigma_f}{\mu_{hnf}/\mu_f}(1-\xi_2) - k_p\frac{\mu_{hnf}/\mu_f}{\mu_{hnf}/\mu_f}(1-\xi_2) - 1, \tag{15}$$

$$\xi\xi_2 = \frac{\left.\begin{matrix} -4R_d\{1+(\theta_w-1)\xi_4\}^2(\theta_w-1)\xi_5^2 - \dfrac{(\rho c_p)_{hnf}}{(\rho c_p)_f} f\theta' \\ -\left\{\dfrac{\mu_{hnf}}{\mu_f}Ecf''^2 + \dfrac{\sigma_{hnf}}{\sigma_f}MEc(1-f')^2\right\} \end{matrix}\right\}}{\left\{\frac{k_{hnf}}{k_f} + \frac{4}{3}R_d\{1+(\theta_w-1)\xi_4\}^3\right\}}, \tag{16}$$

$$\left.\begin{matrix} \xi_1(0) = S,\ \xi_2(0) = \chi,\ \xi_4(0) = 1 \\ \xi_2(\infty) = 1,\ \xi_4(\infty) = 0 \end{matrix}\right\}. \tag{17}$$

5 Conclusion

The goal of the current research is to identify the multiple solutions for the magneto-hybrid nanofluid flow due to a shrinking surface. Additionally, the incorporated consequences of Ohmic heating and non-linear thermal radiation over a convectively heated surface are discussed comprehensively through graphical structures. In this study, multiple solutions occur for various ranges of the shrinking parameter. This research can be summarized in the following way:

- The existence of a shrinking surface promotes the discovery of dual solutions.
- It may be possible to decrease the flow velocity and raise the flow temperature by using higher joule heating and viscous dissipation effects.
- For large values of the Biot number, the temperature distribution and thermal transport rate are more prominent.
- The suction parameter reduces the fluid velocity in the upper branch, while it is enhanced in the lower branch.
- In a physical stable branch, an increasing magnetic strength raises the skin friction coefficient.

Data availability statement

The original contributions presented in the study are included in the article/Supplementary Materials; further inquiries can be directed to the corresponding author.

Author contributions

MN: conceptualization, validation, writing review, and editing. SA: Conceptualization. ZW: Methodology, software. AA: Validation of results. ET-e: Writing original draft preparation, MY: Helping in review processing.

Acknowledgments

The study was supported by the Princess Nourah Bint Abdulrahman University Researchers Supporting Project number (PNURSP2022R52), Princess Nourah Bint Abdulrahman University, Riyadh, Saudi Arabia.

Conflict of interest

The authors declare that the research was conducted in the absence of any commercial or financial relationships that could be construed as a potential conflict of interest.

Publisher's note

All claims expressed in this article are solely those of the authors and do not necessarily represent those of their affiliated organizations, or those of the publisher, the editors, and the reviewers. Any product that may be evaluated in this article, or claim that may be made by its manufacturer, is not guaranteed or endorsed by the publisher.

References

1. Liu MS, Lin MCC, Huang IT, Wang CC. Enhancement of thermal conductivity with carbon nanotube for nanofluids. *Int Commun Heat Mass Transfer* (2005) 32(9):1202–10. doi:10.1016/j.icheatmasstransfer.2005.05.005

2. Choi SUS. Enhancing thermal conductivity of fluids with nanoparticles. *ASMEPublications-Fed* (1995) 231:99–106.

3. Tiwari RK, Das MK. Heat transfer augmentation in a two-sided lid-driven differentially heated square cavity utilizing nanofluids. *Int J Heat Mass Transf* (2007) 50(9-10):2002–18. doi:10.1016/j.ijheatmasstransfer.2006.09.034

4. Karvelas E, Liosis C, Benos L, Karakasidis T, Sarris I. Micromixing efficiency of particles in heavy metal removal processes under various inlet conditions. *Water* (2019) 11(6):1135. doi:10.3390/w11061135

5. Benos LT, Karvelas EG, Sarris IE. A theoretical model for the magnetohydrodynamic natural convection of a CNT-water nanofluid incorporating a renovated Hamilton-Crosser model. *Int J Heat Mass Transf* (2019) 135:548–60. doi:10.1016/j.ijheatmasstransfer.2019.01.148

6. Al-Kouz W, Abderrahmane A, Shamshuddin MD, Younis O, Mohammed S, Bég OA, et al. Heat transfer and entropy generation analysis of water-Fe3O4/CNT hybrid magnetic nanofluid flow in a trapezoidal wavy enclosure containing porous media with the Galerkin finite element method. *Eur Phys J Plus* (2021) 136(11): 1184. doi:10.1140/epjp/s13360-021-02192-3

7. Song YQ, Obideyi BD, Shah NA, Animasaun IL, Mahrous YM, Chung JD. Significance of haphazard motion and thermal migration of alumina and copper nanoparticles across the dynamics of water and ethylene glycol on a convectively heated surface. *Case Stud Therm Eng* (2021) 26:101050. doi:10.1016/j.csite.2021.101050

8. Ishtiaq B, Nadeem S. Theoretical analysis of Casson nanofluid over a vertical exponentially shrinking sheet with inclined magnetic field. *Waves in Random and Complex Media* (2022) 1–17. doi:10.1080/17455030.2022.2103206

9. Sarris IE, Kassinos SC, Carati D. Large-eddy simulations of the turbulent Hartmann flow close to the transitional regime. *Phys Fluids (1994)* (2007) 19(8): 085109. doi:10.1063/1.2757710

10. Riaz A, Ellahi R, Sait SM. Role of hybrid nanoparticles in thermal performance of peristaltic flow of Eyring–Powell fluid model. *J Therm Anal Calorim* (2021) 143(2):1021–35. doi:10.1007/s10973-020-09872-9

11. Raja MAZ, Shoaib M, Tabassum R, Khan MI, Gowda RP, Prasannakumara BC, et al. Intelligent computing for the dynamics of entropy optimized nanofluidic system under impacts of MHD along thick surface. *Int J Mod Phys B* (2021) 35(26): 2150269. doi:10.1142/s0217979221502696

12. Shamshuddin MD, Eid MR. Magnetized nanofluid flow of ferromagnetic nanoparticles from parallel stretchable rotating disk with variable viscosity and thermal conductivity. *Chin J Phys* (2021) 74:20–37. doi:10.1016/j.cjph.2021.07.038

13. Riaz A, Khan SUD, Zeeshan A, Khan SU, Hassan M, Muhammad T. Thermal analysis of peristaltic flow of nanosized particles within a curved channel with second-order partial slip and porous medium. *J Therm Anal Calorim* (2021) 143(3): 1997–2009. doi:10.1007/s10973-020-09454-9

14. Sowmya G, Gireesha BJ, Animasaun IL, Shah NA. Significance of buoyancy and lorentz forces on water-conveying iron (III) oxide and silver nanoparticles in a rectangular cavity mounted with two heated fins: heat transfer analysis. *J Therm Anal Calorim* (2021) 144(6):2369–84. doi:10.1007/s10973-021-10550-7

15. Sabu AS, Mackolil J, Mahanthesh B, Mathew A. Reiner-Rivlin nanomaterial heat transfer over a rotating disk with distinct heat source and multiple slip effects. *Appl Math Mech* (2021) 42(10):1495–510. doi:10.1007/s10483-021-2772-7

16. Mahanthesh B, Shashikumar NS, Lorenzini G. Heat transfer enhancement due to nanoparticles, magnetic field, thermal and exponential space-dependent heat source aspects in nanoliquid flow past a stretchable spinning disk. *J Therm Anal Calorim* (2021) 145(6):3339–47. doi:10.1007/s10973-020-09927-x

17. Yasir M, Ahmed A, Khan M. Carbon nanotubes based fluid flow past a moving thin needle examine through dual solutions: Stability analysis. *J Energ Storage* (2022) 48:103913. doi:10.1016/j.est.2021.103913

18. Umavathi JC, Patil SL, Mahanthesh B, Bég OA. Unsteady squeezing flow of a magnetized nano-lubricant between parallel disks with Robin boundary conditions. *Proc Inst Mech Eng N: J Nanomater Nanoengineering Nanosystems* (2021) 235(3-4): 67–81. doi:10.1177/23977914211036562

19. Salawu SO, Shamshuddin MD, Bég OA. Influence of magnetization, variable viscosity and thermal conductivity on Von Karman swirling flow of H2O-FE3O4 and H2O-Mn-ZNFe2O4 ferromagnetic nanofluids from a spinning DISK: Smart spin coating simulation. *Mater Sci Eng B* (2022) 279:115659. doi:10.1016/j.mseb.2022.115659

20. Yasir M, Hafeez A, Khan M. Thermal conductivity performance in hybrid (SWCNTs-CuO/Ehylene glycol) nanofluid flow: Dual solutions. *Ain Shams Eng J* (2022) 13(5):101703. doi:10.1016/j.asej.2022.101703

21. Gowda RJP, Kumar RN, Prasannakumara BC. Two-phase Darcy-Forchheimer flow of dusty hybrid nanofluid with viscous dissipation over a cylinder. *Int J Appl Comput Math* (2021) 7(3):1–18. doi:10.1007/s40819-021-01033-2

22. Kumar RN, Gowda RP, Abusorrah AM, Mahrous YM, Abu-Hamdeh NH, Issakhov A, et al. Impact of magnetic dipole on ferromagnetic hybrid nanofluid flow over a stretching cylinder. *Phys Scr* (2021) 96(4):045215. doi:10.1088/1402-4896/abe324

23. Hou E, Wang F, Khan MN, Ahmad S, Rehman A, Almaliki AH, et al. Flow analysis of hybridized nanomaterial liquid flow in the existence of multiple slips and Hall current effect over a slendering stretching surface. *Crystals (Basel)* (2021) 11(12):1546. doi:10.3390/cryst11121546

24. Ferdows M, Shamshuddin MD, Salawu SO, Reza M. Computation of heat transfer in magnetised Blasius flow of nano-fluids with suspended carbon nanotubes through a moving flat plate. *Int J Ambient Energ* (2022) 1–9. doi:10.1080/01430750.2022.2075933

25. Animasaun IL, Shah NA, Wakif A, Mahanthesh B, Sivaraj R, Koriko OK. *Ratio of momentum diffusivity to thermal diffusivity: introduction, meta-analysis, and scrutinization*. Florida: CRC Press (2022).

26. Yasir M, Sarfraz M, Khan M, Alzahrani AK, Ullah MZ. Estimation of dual branch solutions for Homann flow of hybrid nanofluid towards biaxial shrinking surface. *J Pet Sci Eng* (2022) 218:110990. doi:10.1016/j.petrol.2022.110990

27. Hady FM, Ibrahim FS, Abdel-Gaied SM, Eid MR. Radiation effect on viscous flow of a nanofluid and heat transfer over a nonlinearly stretching sheet. *Nanoscale Res Lett* (2012) 7(1):229–13. doi:10.1186/1556-276x-7-229

28. Mahanthesh B, Gireesha BJ, Gorla RSR. Nonlinear radiative heat transfer in MHD three-dimensional flow of water based nanofluid over a non-linearly stretching sheet with convective boundary condition. *J Niger Math Soc* (2016) 35(1):178–98. doi:10.1016/j.jnnms.2016.02.003

29. Shoaib M, Raja MAZ, Sabir MT, Islam S, Shah Z, Kumam P, et al. Numerical investigation for rotating flow of MHD hybrid nanofluid with thermal radiation over a stretching sheet. *Sci Rep* (2020) 10(1):18533–15. doi:10.1038/s41598-020-75254-8

30. Mabood F, Yusuf TA, Khan WA. Cu–Al2O3–H2O hybrid nanofluid flow with melting heat transfer, irreversibility analysis and nonlinear thermal radiation. *J Therm Anal Calorim* (2021) 143(2):973–84. doi:10.1007/s10973-020-09720-w

31. Jamaludin A, Nazar R, Pop I. Mixed convection stagnation-point flow of a nanofluid past a permeable stretching/shrinking sheet in the presence of thermal radiation and heat source/sink. *Energies* (2019) 12(5):788. doi:10.3390/en12050788

32. Yasir M, Khan M. Comparative analysis for radiative flow of Cu–Ag/blood and Cu/blood nanofluid through porous medium. *J Pet Sci Eng* (2022) 215:110650. doi:10.1016/j.petrol.2022.110650

33. Yasir M, Khan M, Sarfraz M, Abuzaid D, Ullah MZ. Exploration of the dynamics of ethylene glycol conveying copper and titania nanoparticles on a stretchable/shrinkable curved object: Stability analysis. *Int Commun Heat Mass Transfer* (2022) 137:106225. doi:10.1016/j.icheatmasstransfer.2022.106225

34. Mahanthesh B. Flow and heat transport of nanomaterial with quadratic radiative heat flux and aggregation kinematics of nanoparticles. *Int Commun Heat Mass Transfer* (2021) 127:105521. doi:10.1016/j.icheatmasstransfer.2021.105521

35. Gowda RJP, Kumar RN, Jyothi AM, Prasannakumara BC, Sarris IE. Impact of binary chemical reaction and activation energy on heat and mass transfer of marangoni driven boundary layer flow of a non-Newtonian nanofluid. *Processes* (2021) 9(4):702. doi:10.3390/pr9040702

36. Abdelmalek Z, Khan SU, Waqas H, Riaz A, Khan IA, Tlili I. A mathematical model for bioconvection flow of Williamson nanofluid over a stretching cylinder featuring variable thermal conductivity, activation energy and second-order slip. *J Therm Anal Calorim* (2021) 144(1):205–17. doi:10.1007/s10973-020-09450-z

37. Rana P, Mackolil J, Mahanthesh B, Muhammad T. Cattaneo-Christov Theory to model heat flux effect on nanoliquid slip flow over a spinning disk with nanoparticle aggregation and Hall current. *Waves in Random and Complex Media* (2022) 1–23. doi:10.1080/17455030.2022.2048127

38. Gowda RJP, Kumar RN, Jyothi AM, Prasannakumara BC, Nisar KS. KKL correlation for simulation of nanofluid flow over a stretching sheet considering magnetic dipole and chemical reaction. *ZAMM - J Appl Math Mech/Z Angew Mathematik Mechanik* (2021) 101(11):e202000372. doi:10.1002/zamm.202000372

39. Riaz A, Zeeshan A, Bhatti MM. Entropy analysis on a three-dimensional wavy flow of eyring–powell nanofluid: a comparative study. *Math Probl Eng* (2021). doi:10.1155/2021/6672158

40. Gowda RJ, Kumar RN, Rauf A, Prasannakumara BC, Shehzad SA. Magnetized flow of sutterby nanofluid through cattaneo-christov theory of heat diffusion and stefan blowing condition. *Appl Nanosci* (2021) 1–10. doi:10.1007/s13204-021-01863-y

41. Khan M, Yasir M, Alshomrani AS, Sivasankaran S, Aladwani YR, Ahmed A. Variable heat source in stagnation-point unsteady flow of magnetized Oldroyd-B fluid with cubic autocatalysis chemical reaction. *Ain Shams Eng J* (2022) 13(3): 101610. doi:10.1016/j.asej.2021.10.005

42. Mabood F, Mackolil J, Mahanthesh BSEP, Rauf A, Shehzad SA. Dynamics of Sutterby fluid flow due to a spinning stretching disk with non-Fourier/Fick heat and mass flux models. *Appl Math Mech* (2021) 42(9):1247–58. doi:10.1007/s10483-021-2770-9

43. Kumar RN, Suresha S, Gowda RJ, Megalamani SB, Prasannakumara BC. Exploring the impact of magnetic dipole on the radiative nanofluid flow over a stretching sheet by means of KKL model. *Pramana - J Phys* (2021) 95(4):180–9. doi:10.1007/s12043-021-02212-y

44. Gowda RP, Mallikarjuna HB, Prasannakumara BC, Kumar RN, Manjunatha PT. Dynamics of thermal Marangoni stagnation point flow in dusty Casson nanofluid. *Int J Model Simul* (2021) 42 (5), 1–9. doi:10.1080/02286203.2021.1957330

45. Abo-Elkhair RE, Bhatti MM, Mekheimer KS. Magnetic force effects on peristaltic transport of hybrid bio-nanofluid (AuCu nanoparticles) with moderate Reynolds number: An expanding horizon. *Int Commun Heat Mass Transfer* (2021) 123:105228. doi:10.1016/j.icheatmasstransfer.2021.105228

46. Hafeez A, Yasir M, Khan M, Malik MY, Alqahtani AS. Buoyancy effect on the chemically reactive flow of Cross nanofluid over a shrinking surface: Dual solution. *Int Commun Heat Mass Transfer* (2021) 126:105438. doi:10.1016/j.icheatmasstransfer.2021.105438

Nomenclature

$\boldsymbol{\alpha_{hnf}}$ thermal diffusivity [m^{2}s^{-1}]

$\boldsymbol{k_{hnf}}$ thermal conductivity [kgmK^{-1}s^{-3}]

$(c_p)_{hnf}$ specific heat [m^{2}s^{-2}K^{-1}]

$\boldsymbol{\mu_{hnf}}$ dynamic viscosity [kgm^{-1}s^{-1}]

$\boldsymbol{\nu_{hnf}}$ kinematic viscosity [m^{2}s^{-1}]

$\boldsymbol{\rho_{hnf}}$ density [kgm^{-3}]

$\boldsymbol{\phi_1}$ Au volume fraction

$\boldsymbol{\phi_2}$ Cu volume fraction

$\boldsymbol{u, v}$ velocity components [ms^{-1}]

$\boldsymbol{T}$ fluid temperature [K]

$\boldsymbol{T_\infty}$ ambient temperature [K]

$\boldsymbol{M}$ magnetic parameter

Pr Prandtl number

$\boldsymbol{R_d}$ radiation parameter

$\boldsymbol{Ec}$ Eckert number

$\boldsymbol{\chi}$ stretching/shrinking parameter

$\boldsymbol{f'}$ dimensionless velocity

$\boldsymbol{\theta}$ dimensionless temperature